scientific reports

Check for updates

OPEN

A novel approach for synthesizing silver nanoparticles with antibacterial and cytotoxic activities using the leaf extract of hydroponically grown *Moringa oleifera*

Anush Aghajanyan[1,2]✉, Marina Timotina[3], Tatevik Manutsyan[1,2], Ani Harutyunyan[1,2], Mikayel Ginovyan[2], Robin Schubert[4], Sofiya Aydinyan[5], Karen Trchounian[1,2], Lilit Gabrielyan[1,2]✉ & Liana Gabrielyan[6,7]

Novel approaches for producing silver nanoparticles (Ag-NPs), which are widely used in biomedicine, biotechnology, and agriculture, are of considerable importance. This study highlights a simple and cost-effective biological method for the synthesis of Ag-NPs using the leaf extract of the hydroponically cultivated *Moringa oleifera* (MOAg-NPs), alongside the analysis of the biosynthesized NPs. One of the advantages of hydroponic cultivation over traditional soil-based methods is that plants are cleaner since they are not in contact with soil and can be cultivated with fewer chemical inputs. For characterization of the biosynthesized MOAg-NPs various methods have been used, such as UV-visible (UV-Vis) spectroscopy, transmission electron microscopy (TEM), X-Ray diffraction (XRD), and Fourier transform infrared (FTIR) spectroscopy. UV-Vis analysis revealed a prominent peak at 465 nm, indicating the synthesis of MOAg-NPs. TEM analysis demonstrated a spherical shape of MOAg-NPs with an average diameter of 10.0 ± 6.0 nm. The XRD pattern displayed Ag peaks at 2θ values corresponding to (111), (200), (220) and (311) reflections. The antibacterial efficacy of MOAg-NPs was assessed against Gram-positive (*Enterococcus hirae*, *Staphylococcus aureus*) and Gram-negative bacteria (*Escherichia coli*), revealing their antibacterial potential at low concentrations. The general inhibitory mechanism of MOAg-NPs focuses on the energy-dependent total and *N*, *N′*-dicyclohexylcarbodiimide (DCCD)-sensitive H^+-fluxes across the bacterial membrane. Moreover, the application of MOAg-NPs resulted in substantial inhibition of HeLa cells growth. Thus, Ag-NPs synthesized using hydroponically grown *M. oleifera* leaf extract exhibited cytotoxicity against cancer cells and antibacterial properties, highlighting their potential use in biomedicine.

Keywords *Moringa oleifera* (Lam.), Silver nanoparticles, Green synthesis, Antibacterial activity, ATPase activity, Cytotoxicity

Nanotechnology is considered as one of the foremost contemporary sciences used in various technologies, and its impact has become increasingly evident in recent times. Over the past few years, this area has drawn increasing attention from various scientific disciplines within the research community. Nanotechnology offers a promising alternative through metal nanoparticles (NPs), which could serve as substitutes for current antibiotic

[1]Department of Biochemistry, Microbiology and Biotechnology, Biology Faculty, Yerevan State University, Yerevan 0025, Armenia. [2]Research Institute of Biology, Yerevan State University, Yerevan 0025, Armenia. [3]Department of Medical Biochemistry and Biotechnology, Russian-Armenian University, Yerevan 0051, Armenia. [4]European X-Ray Free-Electron Laser Facility GmbH, 22869 Schenefeld, Germany. [5]Tallinn University of Technology, Tallinn 19086, Estonia. [6]Department of Physical and Colloids Chemistry, Chemistry Faculty, Yerevan State University, Yerevan 0025, Armenia. [7]Chemical Research Center, Laboratory of Physical Chemistry, Yerevan State University, Yerevan 0025, Armenia. ✉email: a.aghajanian@ysu.am; lgabrielyan@ysu.am

treatments[1,2]. The high surface-to-volume ratio of NPs enables more efficient interaction with bacterial cell membranes. Recently, NPs have also attracted attention for their anticancer activity. NPs can be formed from a variety of substances, including metals and metal oxides[1–4]. Due to their distinctive properties, metal and metal oxide NPs carry considerable significance and hold promise for applications ranging from fundamental research to industrial development. Nanomaterials are used in a wide range of fields, including agriculture, food processing, nanomedicine, and more[2,4–8]. The integration of biological cells and bioresources in NPs production represents an innovative nanotechnological strategy, which has gained increasing attention[4–6]. Metal nanoparticles are produced by various methods, encompassing chemical, physical, and biological approaches. However, it has been observed that NPs mediated by plant extracts are more biocompatible, less toxic, and safer for medical applications compared to those produced using physicochemical methods. The biological method, also known as green synthesis, has become a favourable one offering several advantages, such as environmentally friendliness, cost-effectiveness, and safety considerations, elimination of harmful chemicals, reduction of byproduct waste, and low toxicity of the resulting NPs[7,9–11].

Hence, biological synthesis of NPs using plant extracts, which serve as both reducing and capping agents, represents a promising alternative to chemical and physical methods. The physical properties of nanomaterials, such as particle diameter and morphology, can be altered by modifying the external reaction conditions. However, when synthesizing nanomaterials for certain applications, specific limitations often arise. These limitations include high instability, possible toxic effects and incomplete understanding of the mechanisms of action and reactivity of the produced nanomaterials[9,10,12]. Recently, various biological substrates, such as bacterial components, fungi, and plant extracts have been used in the synthesis of metal and metal oxide-based nanomaterials[4,8]. The plant-mediated synthesis offers a straightforward approach, while the use of microorganisms demands additional steps such as cultivation, leading to a diminished yield in NPs synthesis[4,13]. NPs represent a viable strategy for enhancing the bioavailability of active herbal compounds. The synthesis of metal and metal oxide-based nanomaterials depends on the phytochemical composition of plants, which includes secondary metabolites such as alkaloids, flavonoids, phenols, tannins, ascorbic acids, and various other compounds[7,14,15]. These phytocompounds facilitate the production of metal NPs by reducing metal salt and stabilizing the resulting NPs, enhancing their stability and biocompatibility, as well as antioxidant and antibacterial activity[8,15–18]. The therapeutic effects of natural products and metal NPs have been demonstrated in managing a variety of metabolic and infectious disorders, including those related to oxidative stress, bacterial infection, and inflammation[13,19–21]. In our previous studies, green synthesis of Ag-NPs with significant antibacterial potential against conditionally pathogenic bacteria was performed using extracts of medicinal plants *Artemisia annua* and *Stevia rebaudiana*[22,23]. Moreover, Ag-NPs mediated by *S. rebaudiana* extract also altered the energy-dependent H^+-fluxes across the bacterial membrane, even in the presence of *N*, *N*'-dicyclohexylcarbodiimide (DCCD), a specific inhibitor of H^+-translocating transport systems. This observation indicates that the F_OF_1-ATPase, a crucial enzyme of bioenergetics, is a key target of Ag-NPs action[23]. The emergence of NPs as novel antimicrobial agents has stimulated research aimed at addressing superbugs. While numerous papers have been published on the green synthesis of Ag-NPs using plant extracts, there is limited discussion regarding the involvement of phytochemicals or biomolecules, and the mechanisms of NPs formation.

The plant *Moringa oleifera* (MO) is a species native to the Indian subcontinent that is classified within the *Moringaceae* family. Studies have shown that the leaves of *M. oleifera* contain flavonoids such as quercetin, myricetin, kaempferol, and rutin, along with phenolic acids[20]. Additionally, they serve as a rich source of carotenoids, including lutein and β-carotene. It is commonly cultivated due to the diverse applications of green leaves for both edible and medicinal purposes. It is regarded as an excellent food supplement due to its high protein content[20,24–26]. Researchers have studied the nutritional and pharmaceutical properties of *Moringa* plant that is native to diverse regions. As a medicinal plant, it has antioxidant potential as well as anti-inflammatory, anti-microbial and antidiabetic activities, since it contributes to reducing blood glucose levels[20,26,27]. Therefore, using various part of soil-growth *Moringa* for the synthesis of Ag-NPs is a well-founded choice to evaluate the influence of various biomolecules on the size, shape, and antibacterial properties of the nanoparticles[13,28,29]. There is limited literature on the synthesis of Ag-NPs using hydroponically grown *M. oleifera*. One of the advantages of hydroponic cultivation over traditional soil-based methods is that plants grow faster because nutrients are directly delivered to the roots in a readily available form. Additionally, hydroponic cultivation provides complete control over nutrients, water, light, temperature, and pH. These systems often used in controlled environments, enable year-round yields, regardless of climate or season. Hydroponically grown plants are also cleaner since they are not in contact with soil and can be cultivated with fewer chemical inputs. This level of control allows for the optimization of growth conditions, enhancing plant development and yield[30].

The present work aims to establish the synthesis of Ag-NPs by leaf extract from hydroponically cultivated *M. oleifera* (Lam.) and characterize the physicochemical properties, as well as to evaluate the biological activities of these NPs as antibacterial (against multi-drug resistant *Enterococcus hirae*, *Staphylococcus aureus*, *Escherichia coli*) and anticancer agents, and highlight the mechanism of antibacterial action of MOAg-NPs on bacterial membranes.

Results

Green synthesis of MOAg-NPs using *M. oleifera* extract, structural and morphological characterization of MOAg-NPs

The synthesis of MOAg-NPs using an aqueous extract of hydroponically cultivated *M. oleifera* was confirmed by the observable change in the color of the solution, which gradually shifted from yellowish to brown over an hour (Fig. 1). It is widely recognized that Ag-NPs exhibit brown color attributed to their excitation of surface plasmons within the wavelength range of 400–500 nm[23,26,31]. Hence, the color change of the solution indicates the synthesis of MOAg-NPs. This suggests that the aqueous extract of *M. oleifera* promotes the formation of NPs

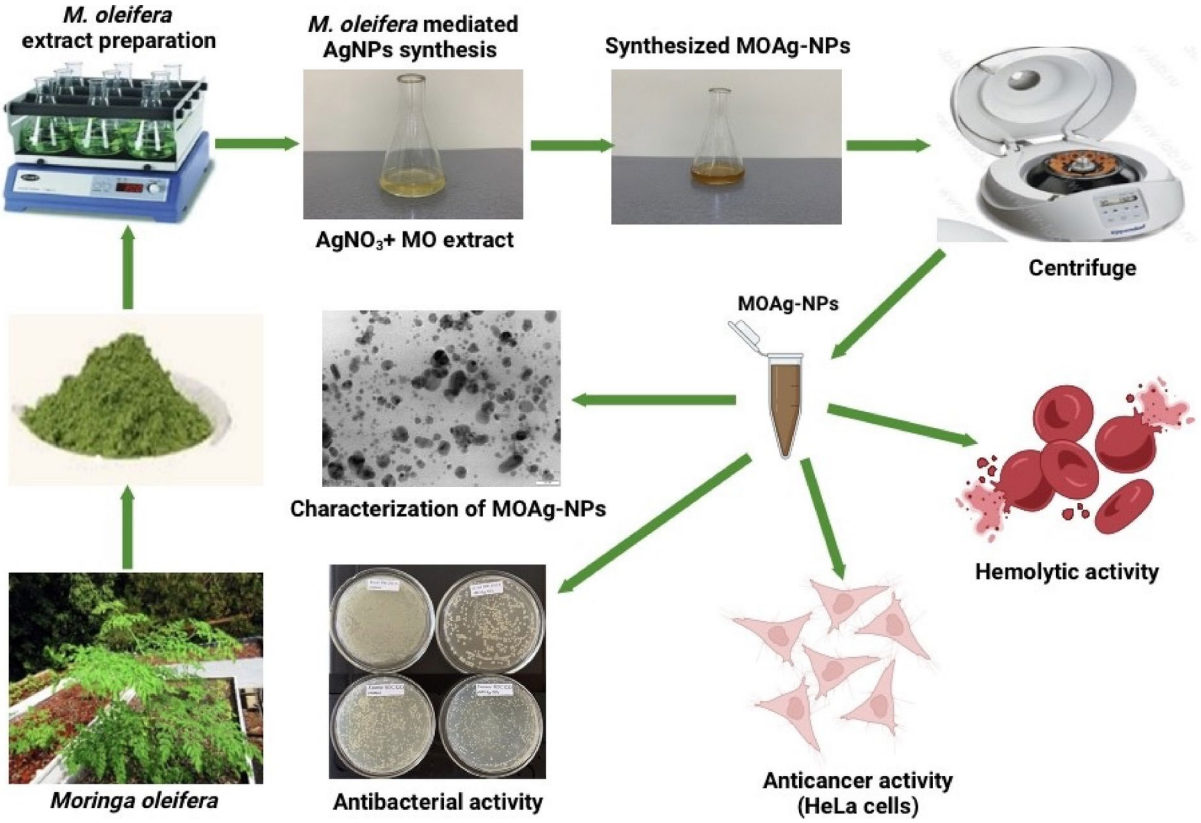

Fig. 1. Schematic illustration of the green synthesis, characterization, and biological activities of MOAg-NPs.

and possesses the capacity for reducing metal ions. Optical absorption spectroscopy of Ag-NPs is a frequently used technique for determining the formation and stability of these nanoparticles. The presence of MOAg-NPs in the reaction mixture was confirmed by UV-Vis spectroscopy, which indicated the characteristic surface plasmon resonance band (SPR). After the incubation period and color change, the UV-Vis spectrum revealed a prominent SPR peak at 465 nm, which is indicative of the presence of Ag-NPs (Fig. 2). The results obtained are consistent with findings reported in other studies[26,32].

Further characterization of the MOAg-NPs was performed using Transmission Electron Microscopy (TEM), which provided detailed information on their size and morphology[19,21,32]. TEM was chosen for this analysis because it allows for accurate measurement of nanoparticles size, free from the bias introduced by larger particles that can affect dynamic light scattering methods. In addition to size determination, TEM also reveals crucial insights into particle morphology, an essential factor in optimizing nanoparticle synthesis processes. The results showed that the MOAg-NPs predominantly exhibited a spherical shape, with particle sizes ranging from 5 nm to approximately 50 nm, and an average diameter of 10.0 ± 6.0 nm (Fig. 3A, B). The particle size has been determined from the TEM image by automated image recognition using NIS-Elements AR software. In addition to the spherical morphology, some nanoparticles showed an elongated shape, indicating a potential anisotropic growth during synthesis. The TEM images revealed that the nanoparticles exhibited a smooth, homogenous surface with no obvious irregularities, suggesting a well-formed, uniform structure (Fig. 3A). The distinct lattice fringes, observable as inhomogeneities in the particle contrast, hinted at their crystalline nature, with contrast variations arising from the orientation of the crystal lattice relative to the electron beam.

The FTIR spectra were analyzed to understand the chemical composition and functional groups. In particular, FTIR analysis was conducted to identify the key biomolecules present in the aqueous extract of *M. oleifera* responsible for reducing Ag ions, as well as to determine the capping agent responsible for the stability of the synthesized nanoparticles. The FTIR spectra of both *M. oleifera* extract and Ag-NPs in the transmittance mode are shown in Fig. 4A. FTIR analysis of *M. oleifera* extract indicates the presence of various intense bands at 3366, 2931, 1612, 1412, 1099, and 605 cm^{-1}, as well as some weak bands or shoulders at 1514, 1270, and 785 cm^{-1}, which can be assigned to the fundamental vibrational modes of different functional groups of organic molecules contained in *M. oleifera*. The changes in the position and intensity of the above-mentioned vibrational bands in the FTIR spectrum of Ag-NPs confirm the involvement of various functional groups of organic compounds of *M. oleifera* in the formation of nanoparticles.

A broad intense absorption band at 3366 cm^{-1}, which is mainly attributed to the O – H stretching vibrations of hydroxyl functional groups of alcohols, and phenols, shifts to 3285 cm^{-1} due to the stretching of OH bond or its participation in the formation of hydrogen bonds (Fig. 4A). The absorption peak at 2931 cm^{-1} with two weak shoulders becomes more pronounced in the FTIR spectrum of Ag-NPs and is observed at 2959,

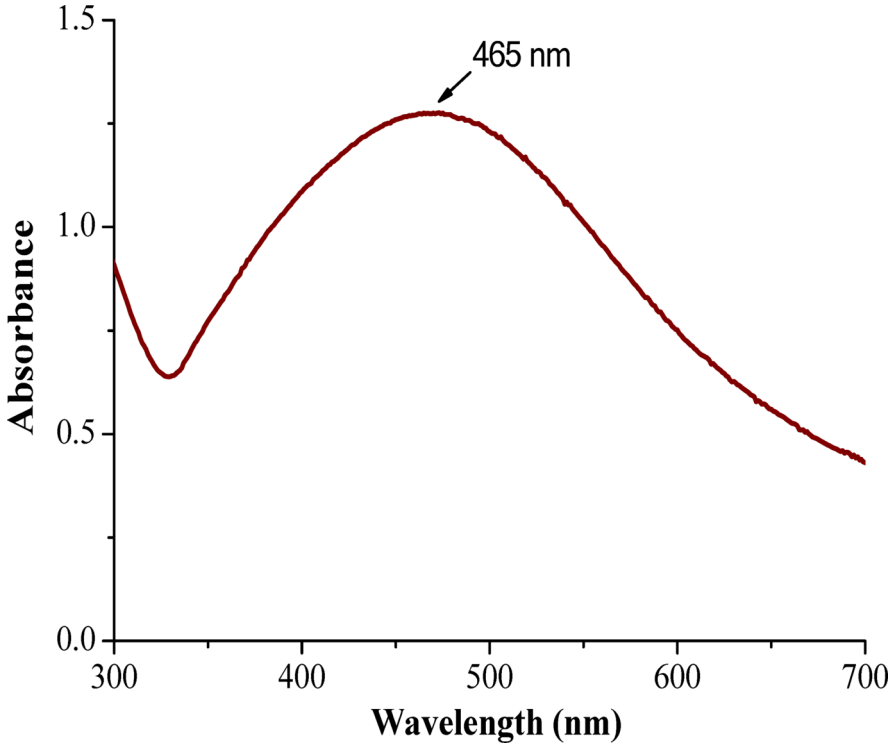

Fig. 2. UV-Vis spectrum of MOAg-NPs synthesized using *M. oleifera* leaf extract.

2920, and 2852 cm^{-1}, indicating the asymmetric and symmetric stretching vibrations of CH_3 or CH_2 groups, respectively[21,33,34]. A pair of strong absorption bands at 1612 and 1412 cm^{-1} are assigned to C = C stretching vibration in the aromatic ring. The original absorption peaks exhibit a blue shift up to 1644 cm^{-1} in the sample of Ag-NPs indicating that the aromatic ring due to the interaction with the nanoparticle surface gets a more rigid structure.

The representative peak at 1099 cm^{-1} can be attributed to the C-O stretching vibration of alcohol, ether or ester. The number of weak absorption peaks in the wavenumber range from 924 to 605 cm^{-1} is quite difficult to interpret, but they are mainly owing to bending vibrations of O-H, aromatic and aliphatic C-H, and C = C groups. The analysis of the FTIR spectrum of Ag-NPs in this range shows that the low-wavenumber peaks exhibit some shifts compared to *M. oleifera*, indicating the involvement of functional groups of biomolecules in the process of nanoparticles formation. The peak observed at 1384 cm^{-1} is possibly due to the symmetrical stretching vibration of the nitro groups. Thus, the change in all absorption bands in the spectrum of Ag-NPs directly confirms the responsibility of *M. oleifera* biomolecules in the process of nanoparticles formation and stabilization.

The XRD analysis confirmed the crystallinity of Ag/AgCl nanoparticles (NPs) with a face-centered cubic (fcc) structure[11,35]. The XRD pattern of MOAg-NPs exhibited distinct diffraction peaks corresponding to silver (Ag) at 2θ values of 38.24° (111), 44.42° (200), 64.64° (220), and 77.55° (311) (Fig. 4B), consistent with the standard reference for fcc silver (PDF#65-2871, JCPDS/ICDD). Additionally, the XRD analysis indicated the presence of 39.4 wt% AgCl, alongside the primary phase of 60.6 wt% Ag, in the *M. oleifera* extract-synthesized samples (Fig. 4B). The calculated lattice constant (a = b = c = 4.0877 Å) closely matched the standard value (4.0862 Å) for silver. Rietveld refinement estimated the crystallite size of silver to be approximately 125 nm, with a lattice strain of 0.445% (Fig. 4B). The formation of AgCl in the form of chlorargyrite within the MOAg-NPs is attributed to the interaction between silver and chloride ions present in the phytochemical extract. Similar observations were reported by Mohammed and Hawar[36], who described the formation of Ag and Ag/AgCl NPs via green synthesis using soil *M. oleifera* leaves.

Dose-dependent antibacterial activity of Ag-NPs against different bacteria

In the present study MOAg-NPs at concentrations of 10, 25, and 50 µg/mL were tested against three bacterial species: *Escherichia coli* BW25113, *Enterococcus hirae* ATCC9790, and *Staphylococcus aureus* MDC5233. In this study, the specific growth rates of these bacteria, cultivated in the presence of biogenic MOAg-NPs were examined, and the antibacterial effect of biogenic MOAg-NPs was determined. Bacterial growth rates in the presence of MOAg-NPs were assessed over 6 h, and the results are shown in Fig. 5. In summary, the results suggest that MOAg-NPs exhibit a significant inhibitory effect on the growth of all tested bacteria. The specific growth rate of bacteria showed concentration-dependent variations (Fig. 5A, B,C). Furthermore, MOAg-NPs exhibited a more significant antibacterial effect on the growth rate of Gram-negative *E. coli* (Fig. 5A). At concentrations of MOAg-NPs of 10, 25 and 50 µg/mL inhibition of bacterial growth by 22%, 66% and 72%, respectively, compared to control cells was observed (Fig. 5A). On the other hand, Gram-positive bacteria (*E. hirae* and *S. aureus*) were less

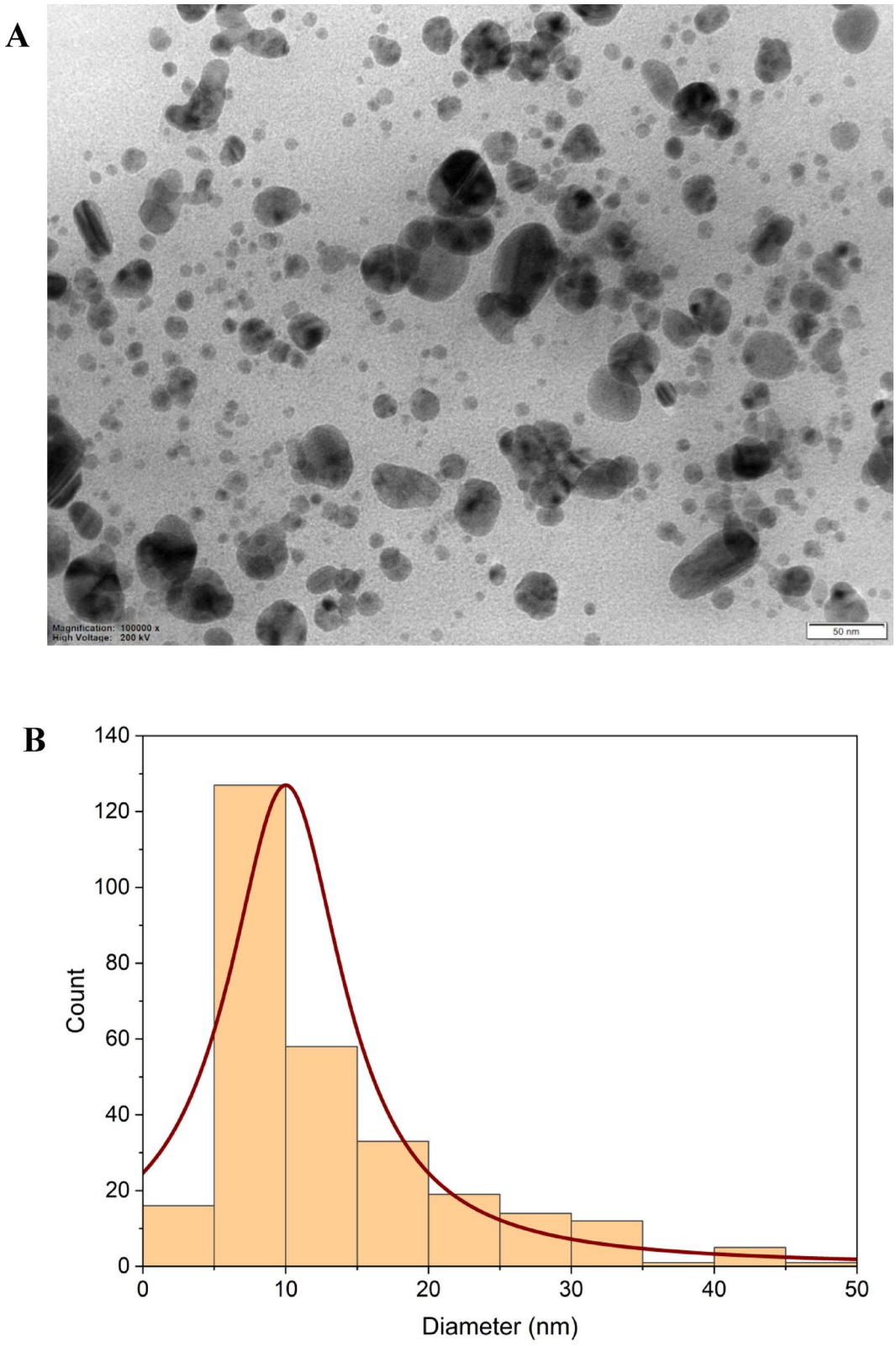

Fig. 3. TEM analysis of the MOAg-NPs synthesized from *M. oleifera* leaf extract. (**A**) TEM image reveals MOAg-NPs have a spherical shape. (**B**) Histography presentation of automated size measurements of MOAg-NPs from TEM images using NIS-Elements AR (Nikon) software and a Lorentzian distribution fit.

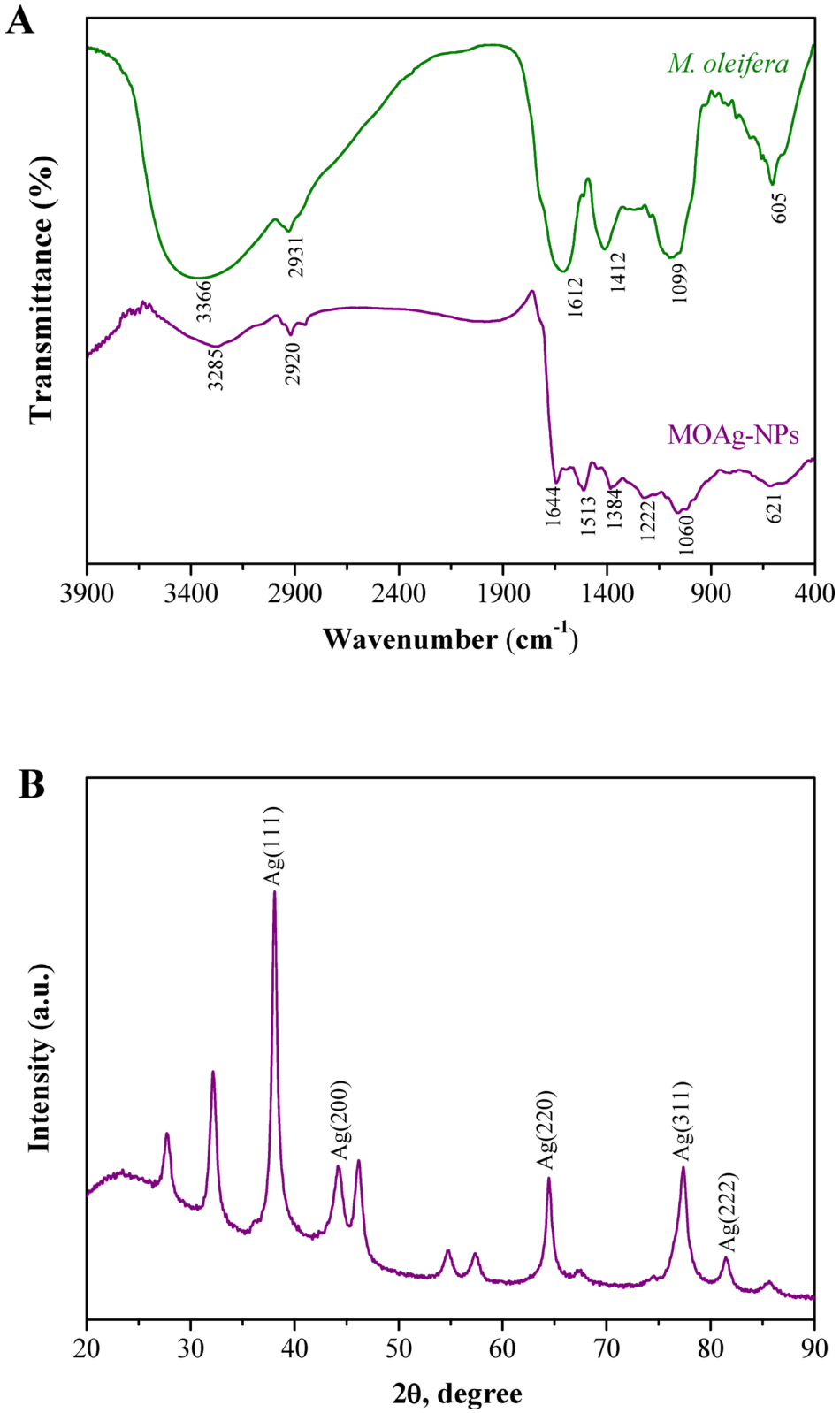

Fig. 4. (**A**) FTIR spectra of *M. oleifera* leaf extract and phyto-mediated MOAg-NPs; (**B**) XRD pattern of the MOAg-NPs.

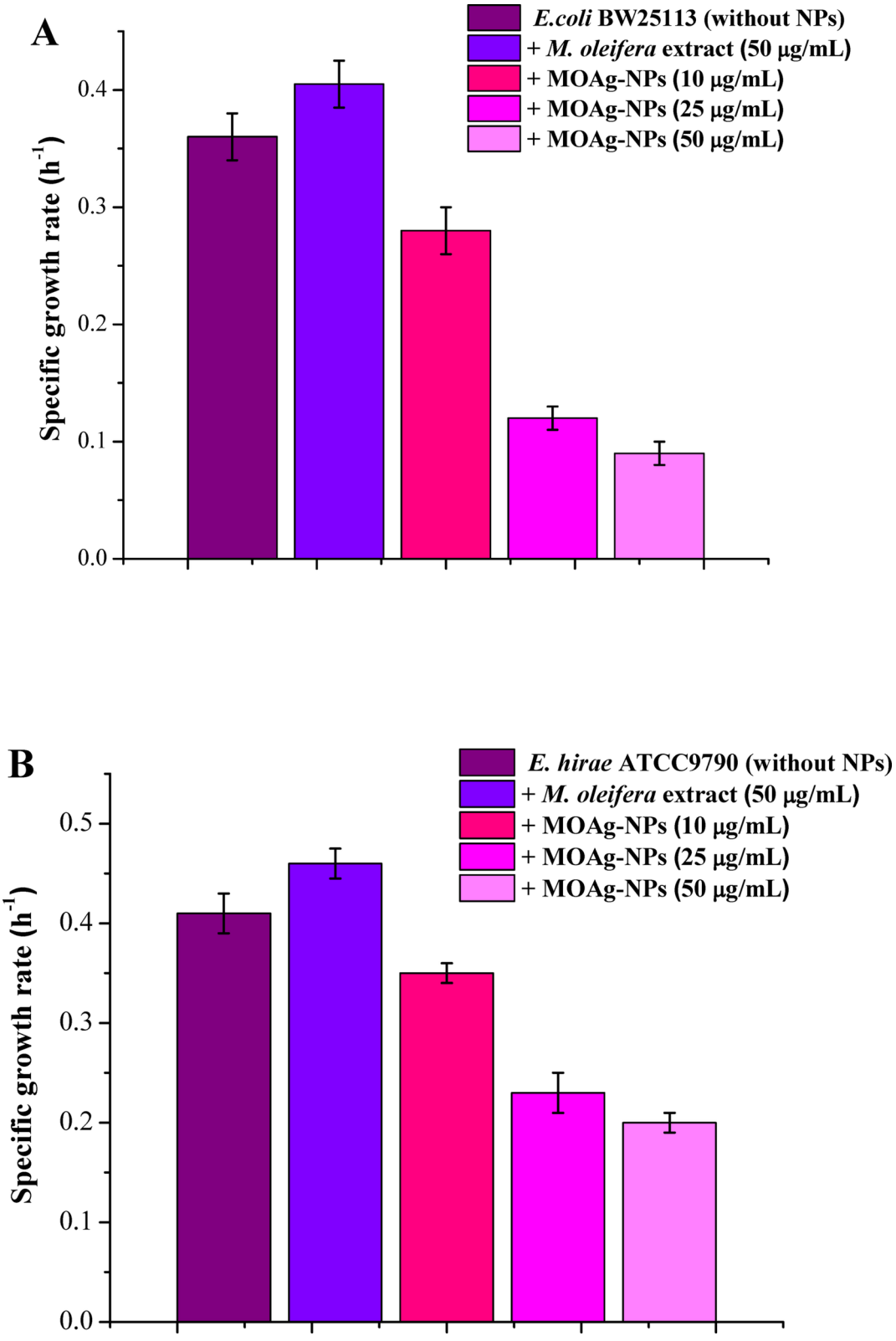

Fig. 5. (**A**) Specific growth rates of *E. coli* BW25113, (**B**) *E. hirae* ATCC9790, (**C**) *S. aureus* MDC5233 strains in the presence of MOAg-NPs synthesized using *M. oleifera* extract. Bacteria cultivated without MOAg-NPs and plant extract were used as controls. Results represent means ± SD ($n = 3$).

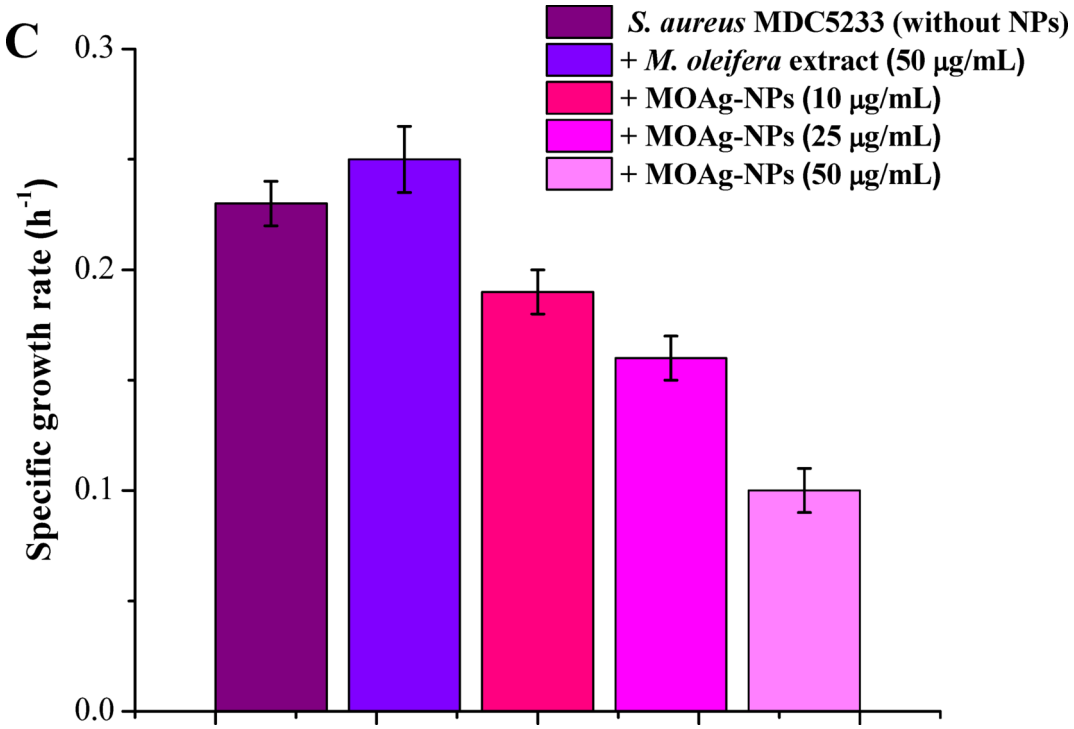

Fig. 5. (continued)

susceptible to the same concentrations of MOAg-NPs. Nevertheless, Gram-positive bacteria also demonstrated dose-dependent effects, as evidenced by 44% and 51% reduction in the growth rate of *E. hirae* at a concentration of 25 and 50 μg/mL; and 30% and 57% reduction in the growth rate of *S. aureus* at the same concentrations of MOAg-NPs (Fig. 5B, C).

The effect of biogenic MOAg-NPs (25 μg/mL) on colony-forming units (CFU) was determined. CFU of Gram-negative *E. coli* decreased by ~ 60% in the presence of MOAg-NPs, whereas *E. hirae* and *S. aureus* exhibited a reduction of ~ 40% and ~ 30%, respectively (Fig. 6A, B). No effect of *M. oleifera* extract at the same concentration on bacterial CFUs was observed. Based on the data, Gram-positive bacteria exhibited lower sensitivity to MOAg-NPs compared to Gram-negative *E. coli*. Therefore, the biosynthesized MOAg-NPs demonstrated antibacterial activity against the tested bacteria. This indicates that MOAg-NPs, due to their diverse mechanisms of penetration through the bacterial cell wall of Gram-positive and Gram-negative bacteria, exhibit promising potential as antibiotic agents and hold promise for future biomedical applications.

The effects of MOAg-NPs on total H^+-fluxes through bacterial membranes and H^+-translocating F_OF_1-ATPase activity

To elucidate the potential mechanisms underlying the antibacterial effects of MOAg-NPs, the energy-dependent H^+-fluxes across the bacterial membrane were assessed. MOAg-NPs elevated the energy-dependent H^+-fluxes in *E. coli*, *E. hirae*, and *S. aureus* by 1.4-, 2-, and 3-fold, respectively, compared to the control group cultivated without MOAg-NPs (Fig. 7). In addition, MOAg-NPs have an impact on the DCCD-dependent H^+-fluxes. DCCD is known to be a specific inhibitor of H^+-translocating transport systems[21,37]. In the presence of DCCD (0.2 mM), the H^+-fluxes in control bacterial cells cultivated without nanoparticles were reduced by 57% for *E. coli*, 42% and 48% for *E. hirae* and *S. aureus*, respectively, compared to the control (Fig. 7). In *E. coli*, the addition of 10 μg/mL MOAg-NPs led to the decrease in DCCD-sensitive H^+-fluxes by 34%, whereas high concentrations (25 and 50 μg/mL) of Ag-NPs completely inhibited the DCCD-sensitive H^+-fluxes. In the case of Gram-positive bacteria, 25 μg/mL MO-AgNPs decreased the DCCD-sensitive H^+-fluxes in *E. hirae* and *S. aureus* by 56% and 44%, respectively. The observed alteration in H^+-fluxes suggests that MOAg-NPs affected bacterial membranes by causing modifications in both membrane structure and permeability via targeting the H^+-translocating F_OF_1-ATPase.

To understand the antibacterial mechanisms of MOAg-NPs, the DCCD-sensitive F_OF_1-ATPase activity was also investigated. Bacterial membrane vesicles were obtained according to[37] to make the ATPase more available to the action of NPs. In the process of membrane vesicles preparation, protoplasts were isolated from Gram-positive *E. hirae* and *S. aureus*, while spheroplasts were obtained from Gram-negative *E. coli*. Bacterial vesicles were treated with 0.2 mM DCCD[36]. Inhibition of DCCD-sensitive F_OF_1-ATPase activity was observed in all three bacterial strains upon the addition of MOAg-NPs (10 μg/mL): 70% inhibition in *E. coli*, 60% in *E. hirae*, and 43% in *S. aureus* (not shown). At high concentrations, MOAg-NPs completely inhibited the DCCD-sensitive ATPase activity. Therefore, MOAg-NPs can impact F_OF_1-ATPase, leading to a reduction in ATPase activity.

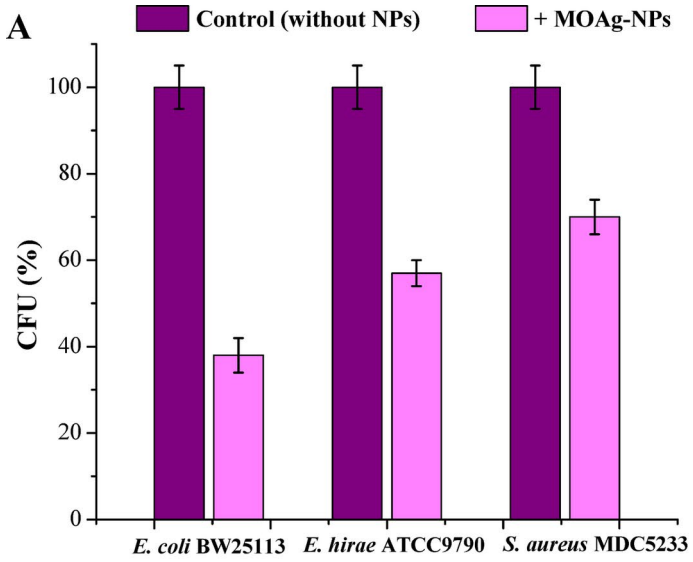

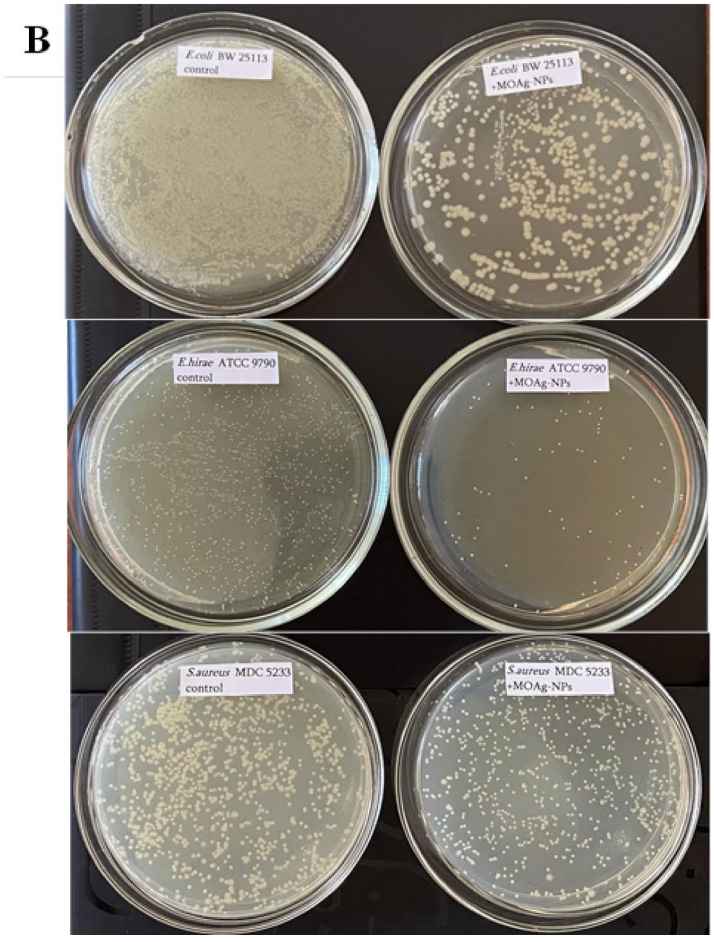

Fig. 6. (**A**) The influence of MOAg-NPs (25 µg/mL) on bacterial colony-forming units (CFU). (**B**) Bacterial colonies were treated with MOAg-NPs synthesized using *M. oleifera* leaf extract against *E. coli* BW25113, *E. hirae* ATCC9790, and *S. aureus* MDC5233. Control samples consisted of bacteria cultivated without Ag-NPs. Results represent means ± SD ($n = 3$).

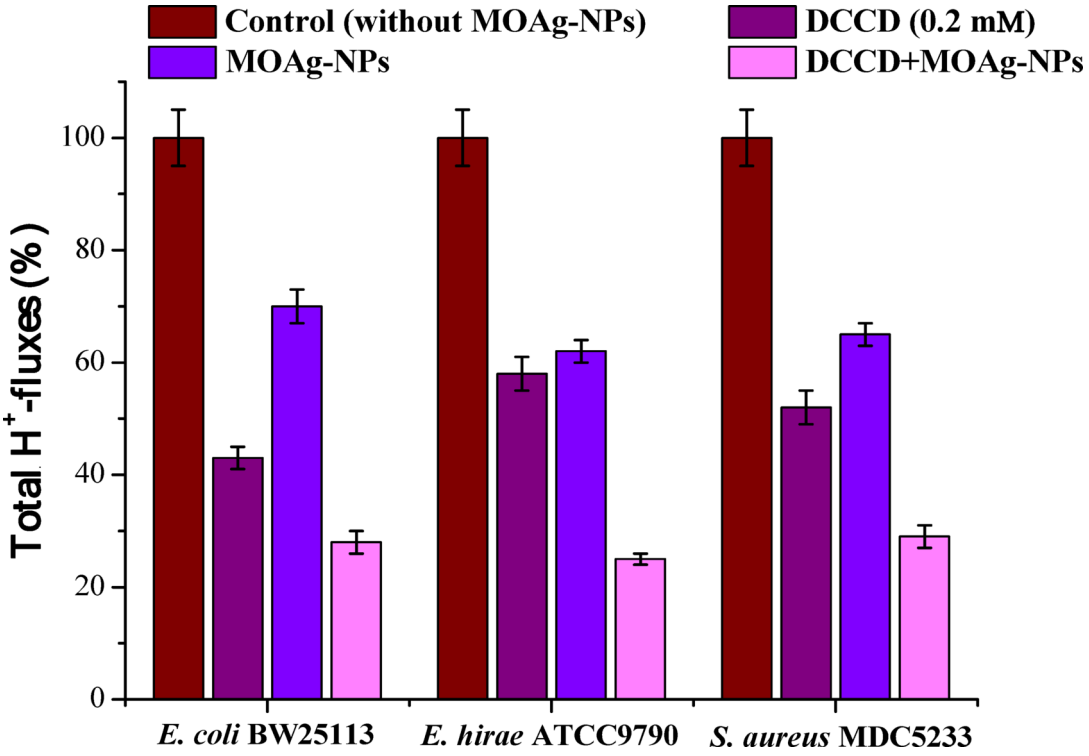

Fig. 7. Alterations in total and DCCD-sensitive H^+-fluxes across the bacterial membranes induced by MOAg-NPs. Concentration of MOAg-NPs for *E. coli* is 10 µg/mL, for *E. hirae* and *S. aureus* is 25 µg/mL. Control samples consisted of bacteria cultured without MOAg-NPs. Results represent means ± SD ($n = 3$).

Growth-inhibitory properties of *M. oleifera* extract and cytotoxic activity of green synthesized MOAg-NPs

The hemolytic activity of MOAg-NPs was determined to assess their biocompatibility with human red blood cells. These NPs showed dose-dependent hemolytic activity against erythrocytes. MOAg-NPs at concentrations of 25 and 50 µg/mL resulted in hemolysis of ~70% and 80%, respectively, while lower concentrations demonstrated no significant effect (Fig. 8A).

In this study, the growth-inhibitory effects of *M. oleifera* extracts and *M. oleifera* green synthesized silver nanoparticles (Ag-NPs) on the growth of HeLa cells were investigated. The efficacy of the extract itself and MOAg-NPs were evaluated at various concentrations and exposure times (4, 24, and 72 h), and the results are presented in Fig. 8B, C. Based on the data obtained, *M. oleifera* extract itself did not significantly inhibit HeLa cells growth, even at the highest concentrations tested (0.5 mg/mL) and the longest exposure times (72 h) (Fig. 8B). In contrast, Ag-NPs synthesized using *M. oleifera* extract exhibited strong growth-inhibitory properties (Fig. 8C).

The data indicate that MOAg-NPs exhibit concentration-dependent cytotoxicity against HeLa cells. At 24 h and 72 h exposure time, NPs induced considerable growth inhibition of HeLa cells even at the lowest concentration tested (6.25 µg/mL). The time-dependent nature of NP-mediated cytotoxicity did not correlate linearly with the concentration dependence. 24 h and 72 h exposure times showed similar growth-inhibitory properties, while the shorter exposure time (4 h) expressed a considerably lower effect. It was clearly evident from the IC_{50} values at different exposure times as well. The IC_{50} values of MOAg-NPs on referring different exposure times were calculated using a nonlinear regression curve fit with a variable slope. The IC_{50} values for 4, 24, and 72 h exposure times were 51.63, 30.47 and 37.02 µg/mL, respectively (Fig. 8C). As can be seen, minimal inhibition was observed at 4 h of exposure, while IC_{50} values for 24 h and 72 h treatments were close to each other. This means that 24 h exposure time is enough for MOAg-NPs to fully express their growth-inhibiting properties. These results suggest that *M. oleifera* green synthesized Ag-NPs have a significant inhibitory impact on HeLa cell proliferation. The results obtained highlight the potential of these NPs to induce sustained inhibitory effects, making them promising candidates for further exploration in anticancer therapy.

Discussion

In recent years, the rate of infectious diseases has increased rapidly due to microbial infections and the emergence of antibiotic drug resistance, which poses significant challenges and affects the overall quality of human health. The occurrence of antibiotic-resistance mechanisms has caused the existing antibacterial drugs to become less effective[38,39]. One perspective strategy to address this issue is to explore natural resources with potential antibacterial properties, which could serve as alternatives to antibiotics. Despite the potent antimicrobial activity of synthetic antibacterial agents, natural resources derived from plants have garnered attention as a potential solution to combat bacterial resistance. These agents can act alone or in conjunction with antibiotics

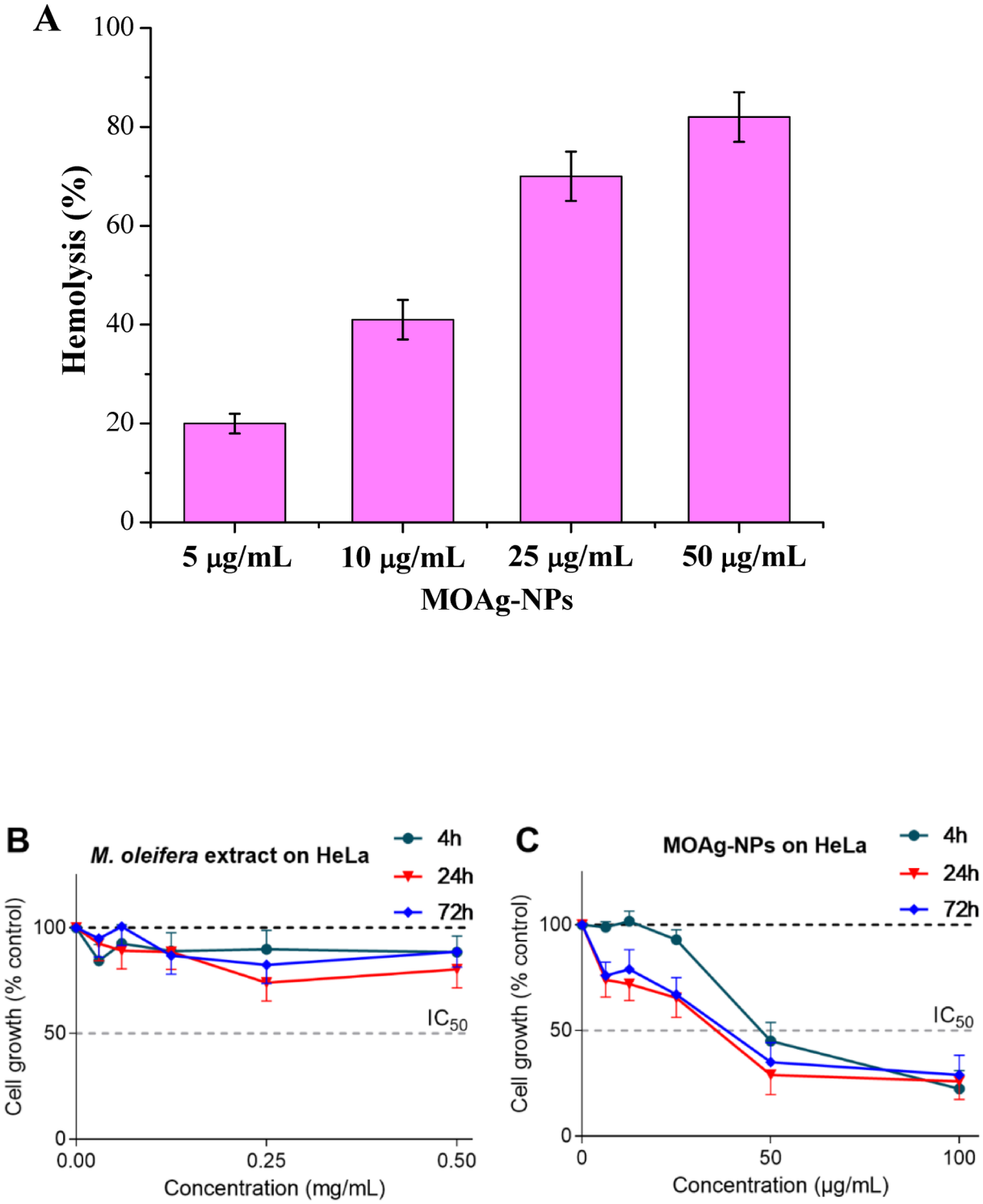

Fig. 8. (**A**) The hemolytic activity of MOAg-NPs. Growth rates of HeLa cells (**B**) treated with *M. oleifera* leaf extract; (**C**) treated with MOAg-NPs for 4, 24, and 72 h. Results represent means ± SD ($n = 3$); SD values did not exceed 15%.

to enhance antibacterial activity against a wide range of bacterial strains. It is well-established that plant-derived compounds have shown promising applications in combating bacterial infections. Furthermore, they can aid restore the clinical efficacy of antibiotics and help prevent the development of resistance[7,40]. Phytocompounds found in plants have demonstrated benefits, including antioxidant, antibacterial, and anticancer activities[4,9,24,25]. Moreover, these phytocompounds can facilitate the synthesis of various NPs with biological activity[8,15,28,29].

Hydroponically cultivated *M. oleifera*-derived Ag-NPs, like other green-synthesized NPs, are nanosized, which enhances their bioavailability, solubility, and absorption, making them suitable for integration into drug delivery systems. Additionally, their high surface-to-volume ratio facilitates efficient interaction with targeted cells or tissues, improving therapeutic efficacy. Integrating MOAg-NPs into existing drug delivery systems can optimize controlled drug release, increase drug stability, and minimize side effects. Moreover, combining MOAg-NPs with conventional drugs in a single delivery system may produce synergistic antimicrobial or anticancer effects, while potentially reducing the required dosage of standard therapies. Furthermore, their potential for multifunctional applications, such as targeting drug-resistant pathogens and cancer cells, makes them a promising addition to advanced therapeutic strategies.

The observed antibacterial activity is determined by key factors such as the choice of raw materials used in NPs derivation as well as their size and shape. It is worthwhile to mention that the synthesis method employed in our study is environmentally friendly, as it utilizes natural sources as reducing and stabilizing agents. Among other NPs, Ag-NPs represent an alternative to combat effectively microbial drug resistance. Due to their versatile properties, such as high stability and good conductivity, Ag-NPs have been extensively used in various fields, particularly in biomedicine and biotechnology[2,11,19,32]. As a result of the ability of NPs to target bacterial cells through multiple pathways, it is difficult for bacteria to survive in the presence of Ag-NPs. Several studies have reported that Ag-NPs synthesized using plant extracts displayed strengthened antibacterial activity against many pathogens[12,28].

Previously, we demonstrated that Ag-NPs synthesized using hydroponically grown medicinal plants, such as *Artemisia annua* and *Stevia rebaudiana* extracts, exhibited significant antibacterial activity[22,23]. However, it should be noted that Ag-NPs synthesized from *Artemisia* were spherical in shape and demonstrated antibacterial effects on the growth of the same bacterial strains only at higher concentrations (100 µg/mL)[22]. In contrast, Ag-NPs synthesized from *Stevia* had an irregular shape and showed a more pronounced antibacterial effect at lower concentration (10 µg/mL) against *E. coli*, while higher concentrations (25 and 50 µg/mL) were needed to affect *E. hirae* and *S. aureus*[23]. Thus, Ag-NPs synthesized from medicinal plants appear to be more susceptible to Gram-negative bacteria as compared to Gram-positive bacteria.

Leaves of medicinal plant *Moringa* contain a range of essential phenols, amino acids, proteins, vitamins, and carbohydrates, which possess diverse bioactivities[20,24,25]. This plant has been effectively used for the synthesis of various nanoparticles with biological activities[13,28,29]. Bindhu with co-workers confirmed that Ag-NPs synthesized using soil-grown *M. oleifera* flowers (spherical NPs with an average size of 8 nm) exhibited antimicrobial activity against *Klebsiella pneumoniae* and *S. aureus*[13]. They hypothesized that the presence of bioactive compounds in the extract facilitated the reduction of Ag-NPs during the synthesis. Kiran with co-authors demonstrated that Au-NPs synthesized from soil-grown *M. oleifera* leaves exhibited antioxidant and anticancer properties[28]. *M. oleifera*-derived Au-NPs exhibit cytotoxicity against MCF-7 cell lines with an IC_{50} value of 67.92 µg/mL. Ezhilarasi and co-workers reported that NiO-NPs prepared using *M. oleifera* leaf extract showed cytotoxic activity against colon cancer HT-29 cell lines[29]. Moreover, NiO-NPs demonstrated significant antibacterial activity against *Streptococcus pneumonia* and *S. aureus*.

In our experiments, hydroponically grown *M. oleifera*-mediated Ag-NPs exhibited an antibacterial effect against *E. coli* and *S. aureus* at low concentrations of 10 and 50 µg/mL, respectively. In contrast, Mohammed and Hawar[36] reported that soil-grown *M. oleifera* leaf extract-derived Ag-NPs inhibited the growth of *E. coli* and *S. aureus* at concentrations of 600 and 1000 µg/mL, respectively. Moreover, MOAg-NPs were smaller (~ 10 nm) compared to those obtained from soil-grown *M. oleifera* (50–60 nm) reported by Mohammed and Hawar[36]. The phytochemical components present in hydroponically cultivated *M. oleifera* can have beneficial effects, acting as both reducing and stabilizing agents during the NPs synthesis process. According to the literature, plant-mediated NPs generally exhibit excellent antibacterial properties and are non-toxic[13,15,32]. Furthermore, MOAg-NPs not only demonstrated strong antibacterial activity but also showed a significant cytotoxic effect against HeLa cells.

The precise mechanism of action of metal NPs is not fully clarified, however, there is considerable evidence that Ag-NPs cause bacterial death by damaging cell structure and disrupting the cell matrix of Gram-positive (*S. aureus* and *E. hirae*) and Gram-negative (*E. coli*) bacterial cells[21,22]. Both metal NPs and natural agents primarily achieve their antibacterial effects by disrupting the bacterial cell membranes. The antimicrobial action of Ag-NPs leads to the rupture of the bacterial cell membrane or the formation of gaps in the outer membrane, resulting in the death of bacterial cells[21,23]. Additionally, Ag-NPs can disrupt bacterial enzymatic processes and induce the formation of reactive oxygen species (ROS), resulting in toxicity to both microbes and host cells and ultimately leading to cell death[2,10,12,16].

When Ag-NPs are absorbed by bacterial cells, NPs bind to the cell wall and plasma membrane, inducing changes in their permeability. Following disruption of the bacterial membrane, cell organelles are also ruptured, resulting in cell lysis. Furthermore, silver ions induce deactivation of respiratory enzymes, which consequently leads to the accumulation of ROS and impedes ATP production[41]. Our findings indicated that Ag-NPs synthesized from *M. oleifera* increased the energy-dependent H^+-fluxes in all tested bacteria. Additionally, these NPs affected the DCCD-dependent H^+-fluxes.

We confirmed that MOAg-NPs affected the bacterial membranes, leading to alterations in both membrane structure and permeability. MOAg-NPs also demonstrated a significant inhibitory effect on H^+-translocating F_OF_1-ATPase, regardless of the bacterial strain type, as observed in all three strains tested. This suggests that F_OF_1-ATPase may be a target through which the antibacterial effect of Ag-NPs is achieved. In aerobic bacteria, the H^+-translocating F_OF_1-ATPase facilitates ATP synthesis during oxidative phosphorylation. In facultative anaerobic bacteria such as *E. coli*, this ATPase operates reversibly depending on growth conditions, whereas, in *E. hirae*, which lacks a respiratory chain, this enzyme only catalyzes the hydrolysis of ATP, linking it to proton gradient formation[42]. Moreover, the H^+-translocating ATPase of *E. hirae* is similar to the well-studied F_OF_1-

ATPase of *E. coli*. Thus, ATP is significantly more crucial for ion transport across the membranes of *Enterococcus* sp. compared to respiring bacteria[42]. In the case of *S. aureus*, ATPase primarily hydrolyzes ATP to maintain the proton gradient under both fermentative and respiratory conditions[43].

The observation that MOAg-NPs inhibit DCCD-sensitive F_OF_1-ATPase activity suggests that these NPs affect the proton translocation mechanism. The bacterial H^+-translocating ATPase is responsible for maintaining the proton gradient across the bacterial membrane, which is crucial for ATP synthesis[1,36]. Inhibition of F_OF_1-ATPase can occur through several potential mechanisms. Ag-NPs are known to interact with bacterial cell membranes, causing alterations in membrane integrity. MOAg-NPs can penetrate the membrane or induce damage by altering the lipid composition and increasing membrane permeability. This disrupts the normal function of membrane proteins, including the H^+-translocating ATPase. By disrupting the structural components of F_OF_1-ATPase or its ability to transfer protons, MOAg-NPs inhibit its capacity to maintain a proton gradient, thereby reducing ATP synthesis and energy-dependent processes in bacterial cells. Ag-NPs can be oxidized and dissolved in aqueous media, releasing Ag ions that can interact with the F_OF_1-ATPase, in particular with the F_O-factor, which is responsible for proton translocation[44].

Thus, MOAg-NPs can damage the membrane, causing proton leakage and collapse of the proton gradient. By disrupting the proton gradient and inhibiting ATP synthesis, Ag-NPs affect cell functions, leading to the disruption of cell homeostasis. The biological significance of this effect is crucial, as it can result in bacterial cell death or significant growth inhibition, making MOAg-NPs effective antibacterial agents.

In our previous research on cyanobacteria *Spirulina platensis*, we found that Ag-NPs synthesized by *Spirulina* had a spherical shape with a hydrodynamic radius of ~29 nm[21]. These nanoparticles demonstrated strong capacity to interact with bacterial membranes, penetrate cells, and effectively inhibit bacterial growth at low concentrations in both Gram-negative (*P. aeruginosa* and *S. typhimurium*) and Gram-positive (*E. hirae* and *S. aureus*) bacteria. These data suggest that the small size of NPs, due to their large surface area and high intracellular penetration, enables them to easily attach to cell membranes, increase membrane permeability, and ultimately lead to cell death.

In the current study, the synthesized MOAg-NPs have a spherical morphology with an average size of 10 nm. As previously mentioned, the effectiveness of Ag-NPs is determined by the morphology and size of the nanoparticles. Due to their larger surface area, smaller-sized Ag-NPs tend to release silver ions, thus exhibiting higher activity compared to larger NPs. Numerous studies have indicated that Ag-NPs smaller than 10 nm exhibit greater antibacterial efficacy and higher cytotoxicity compared to larger ones[13,17,22]. Nanoparticles have been found to result in increased toxicity observed in tumor cells. However, it is crucial to assess the cytotoxicity of nanoparticles on normal cells, as very small nanoparticles are known to exhibit toxicity[32].

Our previous research demonstrates that small Ag-NPs exhibit much greater antimicrobial activity than large Ag-NPs at the same concentrations[21,23]. It is possible that the size of NPs depends on the biomolecules present in the plants. However, further testing of these nanoparticles on drug-resistant or multidrug-resistant bacteria and elucidation of their antifungal activity are required.

According to the literature, metal NPs have exhibited anti-cancer activity against human colon adenocarcinoma and breast carcinoma cell lines, revealing their toxic effects on cancer cells[18,45,46]. Significantly, the NPs disrupt the activity of multidrug resistance transporters found in cancer cells[18,29,45]. Cell-penetrating peptides are commonly used in combination with Ag-NPs to facilitate their intracellular transportation within cancer cells.

The potential mechanisms proposed to explain the anticancer activity of biological nanoparticles include the generation of ROS[2,18,45]. ROS generation plays a crucial role in the anticancer activity of Ag-NPs by inducing oxidative stress in cancer cells. Oxidative stress has the potential to induce an inflammatory reaction that may result in the damage of crucial cell components, such as mitochondria and DNA, disrupting cell functions[29,45]. These effects ultimately result in apoptosis, necrosis, or impaired cell functions[2]. This mechanism is particularly significant for targeting multidrug-resistant cancer cells, as ROS can overcome cell defenses that typically protect these cells from conventional chemotherapy[29,45]. Green synthesized Ag-NPs induced apoptosis in human breast cancer cells[45]. As noted by the authors, apoptosis was dose-dependent and was accompanied by the generation of ROS, leading to mitochondria and DNA damage in cancer cells. Following exposure to Ag-NPs, there is an increase in ROS levels, resulting in cellular toxicity, decreased cell division rate, and damage to cell organelles, which ultimately leads to cell death[18,45,47]. Thus, by inducing oxidative damage, ROS can bypass traditional resistance pathways, making Ag-NPs a promising strategy for overcoming drug resistance in cancer treatment.

The mechanism of action of metal nanoparticles involves the release of ions toxic to pathogens, increased permeability of the bacterial membrane, damage to cell components, and inhibition of DNA replication[1,2,45,47]. In the context of bacteria, smaller, spherical nanoparticles can effectively disrupt membrane integrity and inhibit vital enzymes such as H^+-translocating F_OF_1-ATPase, making them valuable against multidrug-resistant strains. For cancer therapies, strategies that boost nanoparticle-induced ROS generation can help overcome drug resistance by damaging cancer cells at multiple levels (e.g. membranes, mitochondria, and DNA), while simultaneously disrupting multidrug efflux transporters. These properties make them promising candidates for combating drug-resistant pathogens and cancer.

In our study, MOAg-NPs demonstrated significant growth-inhibitory properties on HeLa cells. Our findings suggest that Ag-NPs synthesized from *Moringa oleifera* have potential for further investigation in anticancer therapy. Despite the advantages of green synthesis of nanoparticles and the significant contribution of plant sources to NPs synthesis, it is important to recognize that a full understanding of the detailed mechanism of action during this process remains limited and there are aspects that have yet to be fully explored. More notably, the morphology of NPs derived from different plant sources can vary considerably. The physicochemical parameters of these NPs play a crucial role in determining their overall properties during green synthesis. Therefore, further research is necessary to improve the production of NPs with high consistency for their

potential application as antibacterial or anticancer agents in various fields. Also, additional experiments using normal (non-cancerous) cell lines are important to fully assess the safety profile of MOAg-NPs. These studies will help determine potential off-target effects and establish a therapeutic window that ensures selective toxicity to cancer cells while minimizing toxicity to healthy tissues. Furthermore, in vivo studies are required to confirm both the safety and anticancer efficacy of Ag-NPs, including detailed toxicity profiling, biodistribution analysis, and assessments of the immunological response in animal models.

Conclusion

The outcomes of this work demonstrate that the leaf extract from hydroponically cultivated *M. oleifera* was successfully used to synthesize spherical Ag-NPs with biological activity (Fig. 1). The XRD analysis confirmed the crystallinity of MOAg-NPs, and the FTIR spectrum of these NPs indicated the involvement of biomolecular functional groups in the nanoparticle formation process. The resulting MOAg-NPs exhibited promising antibacterial efficacy at low concentrations against both Gram-positive and Gram-negative bacteria, with Gram-negative bacteria showing greater susceptibility. Notably, MOAg-NPs not only inhibited bacterial growth and CFU counts but also disrupted energy-dependent H^+-fluxes across bacterial membranes. This suggests that the H^+-translocating F_OF_1-ATPase may serve as a key target for their antibacterial action. The MOAg-NPs significantly inhibited HeLa cell growth even at the lowest concentration, suggesting that *M. oleifera*-mediated Ag-NPs have a strong inhibitory effect on HeLa cell proliferation. This approach highlights the potential of plant-based nanotechnology and establishes a foundation for future research on therapeutic applications and environmental implications of biosynthesized nanoparticles.

Methods

Plant material and its growth condition

M. oleifera (Lam.) (authentication number 13755 ERCB) was cultivated using hydroponic methods at the Institute of Hydroponics Problems (NAS, Yerevan, Armenia) (Fig. 1)[27]. The plant sprouts were transferred into classical hydroponic conditions (the seating density is 6 plants/m^2). They were cultivated on volcanic slag particles, which had a diameter ranging from 3 to 15 mm, and supplemented with a nutrient solution. The leaves were harvested during the flowering period, and the dry material was supplied.

Preparation of aqueous extract of *M. oleifera* leaves

The dried leaves of MO were ground into powder using a mortar, and an aqueous extract was prepared as a platform for NPs synthesis (Fig. 1). The powder (5 g) was mixed with 100 mL of deionized water in a 500 mL Erlenmeyer flask, and the solution was shaken for 1 h at 150 rpm and 60 °C. Then, the extract was cooled to room temperature and filtered through Whatman filter paper No. 1 for NPs synthesis.

Synthesis of Ag-NPs using *M. oleifera* extract

Stable MOAg-NPs were synthesized by reducing silver salt solution ($AgNO_3$, 99% purity) with *M. oleifera* extract (Fig. 1). 1 mM $AgNO_3$ aqueous solution was prepared for NPs synthesis. During the synthesis, 9 mL of 1 mM $AgNO_3$ solution was mixed with 1 mL of MO extract solution[22]. The mixture was left at room temperature for 50–60 min under daylight illumination. The reaction mixture of $AgNO_3$ and the extract was a yellowish color. Following NPs synthesis, the solution underwent a color change from light yellowish to dark brown, indicating the reduction of Ag^+ ions ($Ag^+ \rightarrow Ag^0$). Subsequently, the precipitate was separated by centrifugation at 14,000 rpm for 5 min, and the resulting precipitate was resuspended in deionized water for further analysis (Fig. 1).

Physicochemical characteristics of biosynthesized MOAg-NPs

UV/Vis spectra

The bio-reduction of Ag^+ ions and the kinetics of MOAg-NPs formation were confirmed using a UV–Vis spectrophotometer (Genesys 10 S UV-VIS, Thermo Fisher Scientific, and UV 2700, Shimadzu). The optical absorption spectrum and surface plasmon resonance (SPR) peak of Ag-NPs were recorded in the range of 300–700 nm at a resolution of 1 nm.

Transmission Electron microscopy (TEM)

Transmission electron microscopy (TEM) measurements were conducted to reveal the formation of MOAg-NPs and their morphology. 3 µL of the MOAg-NP sample was applied on a glow discharged (Quorum GloCubePlus) carbon-coated formvar copper grid, blotted, and dried[21].

X-Ray diffraction (XRD) and fourier transform infrared (FTIR) spectroscopy analysis

The phase composition of the samples was identified by XRD analysis using a MiniFlex 600 Rigaku Smart Lab SE diffractometer (Rigaku Corporation, Japan, D/teX Ultra 250 1D detector, CuKα radiation, λ = 0.1542 nm, step size of 0.01°) and a PDF-2 database (Ag/PDF#65-2871, AgCl/PDF#31-1238)[21]. The relative content of the existing phases (silver and silver chloride) was estimated by the Rietveld refinement method (S = 1.41, $\chi^2 = 1.99$). The calculated Crystallinity Index (CI) for silver (Ag) based on the XRD data and PDF# 65-2871 is 64.71%, indicating a moderately high degree of crystallinity in the sample (no-peak region 2θ = 10-20° was deduced from the calculation).

FTIR spectroscopy was used to determine characteristic functional groups of *M. oleifera* and obtain information about their involvement in the formation of Ag-NPs. FTIR spectra of both *M. oleifera* extract and Ag-NPs were registered in transmittance mode between 4000 and 400 cm^{-1} with a resolution of 8 cm^{-1} and 32

parallel scans using a Nicolet iS50 FTIR spectrometer (Thermo Fisher Scientific, USA)[21]. The dried sample of *M. oleifera* extract and Ag-NPs were separately mixed with KBr powder in an agate mortar and then the resulting mixtures were compressed into transparent KBr pellets.

Biological activities of biosynthesized MOAg-NPs

Determination of the antibacterial activity of MOAg-NPs

The antibacterial activity of biogenic Ag-NPs was tested against Gram-negative and Gram-positive bacterial species. For this study, the experiments were conducted using *Escherichia coli* BW25113, *Enterococcus hirae* ATCC9790 and *Staphylococcus aureus* MDC5233 (Microbial Depository Center, NAS, Yerevan, Armenia, WDCM803)[21]. The strains were cultivated in peptone, tryptone and Nutrient broth (NB) growth media, respectively, at 37 °C and pH 7.5, with the addition of glucose (2%) as a carbon source. Anaerobic conditions were maintained[21,37]. Bacteria cultivated without Ag-NPs served as a negative control, while the plant extract was employed as a positive control. Bacterial growth was determined using a densitometer (DEN-1B McFarland, Biosan, Latvia) by adding Ag-NPs at concentrations of 10, 25, and 50 µg/mL to the growth media[21]. The specific growth rate (µ) of bacteria was calculated using the formula:

$$\mu = \frac{(\ln OD_t - \ln OD_0)}{\Delta t}$$

where μ is the specific growth rate, OD_t and OD_0 are the final and initial optical density of cells, respectively, and Δt is the time interval during 6 h (exponential growth phase)[21].

Evaluation of bacterial susceptibility to MOAg-NPs

The spread plate technique was employed to evaluate bacterial susceptibility to phyto-mediated Ag-NPs. Sterilized Petri dishes were filled with 30 mL of peptone, tryptone, and NB media, each supplemented with 1.5% w/v bacteriological agar. The bacterial suspension was grown in the presence of MOAg-NPs and then diluted to 10^8 CFU (colony-forming units)/mL. Subsequently, 100 µL of each sample was spread onto the solid growth media. The test organisms were then incubated overnight at 37 °C. The CFU was determined by counting viable colonies as described[21,23].

Determination of total and DCCD-sensitive H^+-fluxes through the bacterial membrane

The mechanisms by which MOAg-NPs affect energy-dependent H^+-fluxes across the bacterial membrane were investigated as described[21]. To elucidate the potential mechanisms of NPs action, 0.2 mM *N*, *N*'-dicyclohexylcarbodiimide (DCCD), an inhibitor of H^+-translocating systems, was introduced. Bacterial cells were incubated with DCCD and MOAg-NPs for 10 min. The H^+-fluxes were assessed based on alterations in ion external activity and quantified as mmol H^+ per minute per 10^{10} cells[37].

Determination of H^+-translocating ATPase activity

For the experiment, membrane vesicles of bacteria were prepared as described[37]. To determine the protein content, the Lowry method was used. H^+-translocating F_OF_1-ATPase activity was defined by the amount of inorganic phosphate (P_i) produced during the reaction using the Taussky and Shorr method[37]. DCCD (0.2 mM) and MOAg-NPs (10 µg/mL) were used in a 10 min incubation of bacterial membrane vesicles. The measurements were recorded by a UV–Vis spectrophotometer (Genesys 10 S UV-Vis-Thermo Fisher Scientific and UV 2700, Shimadzu) at 710 nm[37].

Determination of the hemolytic activity of MOAg-NPs

The hemolytic activity of NPs was determined according to the procedure described[48]. Erythrocytes resistance to MOAg-NPs was measured by the change in the OD_{576} of the erythrocytes suspension by Spectro UV-Vis Auto spectrophotometer (Genesys 10 S UV–VIS-Thermo Fisher Scientific, Shimadzu) and calculated as described[48]. 0.1% Triton X-100 was used as a negative control.

All human blood samples were obtained from healthy volunteers with informed consent from all subjects. The study was conducted following relevant guidelines and regulations, according to the "Human Rights and Biomedicine, Oviedo Convention" (CE, 1997), and was approved by the National Center of Bioethics (Armenia).

Evaluation of cytotoxicity using the MTT assay

The MTT assay was conducted to evaluate the inhibitory effect on the growth of HeLa cells (CCL-2) following exposure to various concentrations of *M. oleifera* extract and MOAg-NPs for 4, 24, or 72 h, as described previously[49]. Three independent experiments were conducted with three technical replicates each. Cells were maintained in Dulbecco's Modified Essential Medium/Nutrient Mixture F-12 Ham (DMEM, Sigma-Aldrich No. D6421) supplemented with 10% Fetal Bovine Serum (FBS, Sigma-Aldrich) and 1x Penicillin-Streptomycin. Cultured cells were routinely screened for mycoplasma contamination using the Universal Mycoplasma Detection Kit (ATCC 30–1012 K™, Monassas, VA, USA). Cells were maintained at 37 ºC under a humidified atmosphere with 5% CO_2 in in a CO_2 incubator (Biosan S-Bt Smart Biotherm). Cytotoxicity was quantified as the percentage of growth inhibition in cells treated with the test plant extract or MOAg-NPs, compared to control cells treated solely with the appropriate volume of solvent (sterile distilled water), the growth of which was considered 100%. The IC_{50} values for MOAg-NPs, across different exposure times, were determined using a nonlinear regression curve fit with a variable slope.

Reagents

All chemicals used in this experiment were of the highest purity. D-glucose, $AgNO_3$, tryptone, and DCCD were purchased from Sigma Aldrich (USA); NB media was purchased from Condalab (Spain); peptone and TRIS (Tris(hydroxymethyl)aminomethane) were purchased from Carl Roth GmbH (Germany).

Statistical analysis

All experiments were conducted at least in triplicate ($n = 3$). The data were presented as the mean ± standard deviation (SD) of the mean. The Student's t-test was chosen for statistical analysis to assess significant differences in experimental data between various series. The significance level of $p \leq 0.05$ was considered to determine statistically significant differences between the mean values.

Data availability

All data generated or analyzed during this study are included in this manuscript.

Received: 2 December 2024; Accepted: 2 May 2025
Published online: 13 May 2025

References

1. Gabrielyan, L., Trchounian, A. Antibacterial activities of transient metals nanoparticles and membranous mechanisms of action. World J. Microbiol. Biotechnol. 35, 162; https://doi.org/10.1007/s11274-019-2742-6 (2019).
2. Srivastava, S., Bhargava, A. Green Nanoparticles: The Future of Nanobiotechnology. 358 p.; https://doi.org/10.1007/978-981-16-7106-7 (Springer, 2022).
3. Bharti, S. Harnessing the potential of bimetallic nanoparticles: exploring a novel approach to address antimicrobial resistance. World J. Microbiol. Biotechnol. 40, 89; https://doi.org/10.1007/s11274-024-03923-1 (2024).
4. Gebre, S.H. Bio-inspired synthesis of metal and metal oxide nanoparticles: the key role of phytochemicals. J. Cluster. Sci. 34, 1–40; https://doi.org/10.1007/s10876-022-02276-9 (2022).
5. Kirubakaran, D., Wahid, J.B.A., Karmegam, N. *et al.* A comprehensive review on the green synthesis of nanoparticles: advancements in biomedical and environmental applications. Biomedical Materials & Devices. https://doi.org/10.1007/s44174-025-00295-4 (2025).
6. Patra, N., Kar, D., Pal, A., Behera, A. Antibacterial, anticancer, anti-diabetic and catalytic activity of bio-conjugated metal nanoparticles. *Adv. Nat. Sci.: Nanosci. Nanotechnol.* **9**, 035001; https://doi.org/10.1088/2043-6254/aad12d (2018).
7. Dewi, M.K., Chaerunisaa, A.Y., Muhaimin, M., Joni, I.M. Improved activity of herbal medicines through nanotechnology. *Nanomaterials (Basel)* **12**, 4073 https://doi.org/10.3390/nano12224073 (2022).
8. Ghasemi, S. et al. Process optimization for green synthesis of silver nanoparticles using *Rubus discolor* leaves extract and its biological activities against multi-drug resistant bacteria and cancer cells. Sci. Rep. 14, 4130; https://doi.org/10.1038/s41598-024-54702-9 (2024).
9. Rocha, V., Ferreira-Santos, P., Aguiar, C., Neves, I.C., Tavares, T. Valorization of plant by-products in the biosynthesis of silver nanoparticles with antimicrobial and catalytic properties. Env. Sci. Poll. Res. 31, 14191–14207; https://doi.org/10.1007/s11356-024-32180-w (2024).
10. Chandraker, S., Kumar, R. Biogenic biocompatible silver nanoparticles: a promising antibacterial agent. BGER 40, 3113–3147; https://doi.org/10.1080/02648725.2022.2106084 (2022).
11. Dhaka, A., Mali, S.C., Sharma, S., Trivedi, R. A review on biological synthesis of silver nanoparticles and their potential applications. Results Chem. 6, 101108. https://doi.org/10.1016/j.rechem.2023.101108 (2023).
12. Salem, S.S., Fouda, A. Green synthesis of metallic nanoparticles and their prospective biotechnological applications: an overview. Biol. Trace Elem. Res. 199, 344–370; https://doi.org/10.1007/s12011-020-02138-3 (2021).
13. Bindhu, M.R., Umadevi, M., Esmail, G.A., Al-Dhabi, N.A., Arasu, M.V. Green synthesis and characterization of silver nanoparticles from *Moringa oleifera* flower and assessment of antimicrobial and sensing properties. J. Photochem. Photobiol. B. Biology 205, 111836; https://doi.org/10.1016/j.jphotobiol.2020.111836 (2020).
14. Manzoor, S.I. et al. Green synthesis of biocompatible silver nanoparticles using *Trillium govanianum* rhizome extract: comprehensive biological evaluation and *in Silico* analysis. Mater. Adv. 6, 682–702; https://doi.org/10.1039/D4MA00959B (2025).
15. Pandey, P.K. et al. Anticancerous and antioxidant properties of fabricated silver nanoparticles involving bio-organic framework using medicinal plant *Blumea lacera*. Chem. Pap. 77, 3603–3617; https://doi.org/10.1007/s11696-023-02723-5 (2023).
16. Chuy, G. et al. Green nanoarchitectonics of silver nanoparticles for antimicrobial activity against resistant pathogen. J. Inorg. Organomet. Polym. Mater. 32, 1213–1222; https://doi.org/10.1007/s10904-021-02162-3 (2021).
17. Shalaby, E.A., Shanab, S.M.M., ElRaheem, W.M.A., Hanafy, E.A. Biological activities and antioxidant potential of different biosynthesized nanoparticles of *Moringa oleifera*. Sci. Rep. 12, 18400; https://doi.org/10.1038/s41598-022-23164-2 (2022).
18. Noorbazargan, H. et al. Anti-cancer & anti-metastasis properties of bioorganic-capped silver nanoparticles fabricated from *Juniperus chinensis* extract against lung cancer cells. AMB Express 11, 61; https://doi.org/10.1186/s13568-021-01216-6 (2021).
19. Chandraker, S.K. et al. Therapeutic potential of biogenic and optimized silver nanoparticles using *Rubia cordifolia* L. leaf extract. Sci. Rep. 12, 8831; https://doi.org/10.1038/s41598-022-12878-y (2022).
20. Peñalver, R., Martínez-Zamora, L., Lorenzo, J.M., Ros, G., Nieto, G. Nutritional and antioxidant properties of *Moringa oleifera* leaves in functional foods. Foods 11, 1107; https://doi.org/10.3390/foods11081107 (2022).
21. Harutyunyan A. et al. Comparative study of physicochemical properties and antibacterial potential of cyanobacteria *Spirulina platensis*-derived and chemically synthesized silver nanoparticles. ACS Omega 9, 29410–29421; https://doi.org/10.1021/acsomega.4c01604 (2024).
22. Aghajanyan, A., Gabrielyan, L., Schubert, R., Trchounian A. Silver ion bioreduction in nanoparticles using *Artemisia annua* L. extract: characterization and application as antibacterial agents. AMB Express 10, 66; https://doi.org/10.1186/s13568-020-01002-w (2020).
23. Timotina, M., Aghajanyan, A., Schubert, R., Trchounian, K., Gabrielyan, L. Biosynthesis of silver nanoparticles using extracts of *Stevia rebaudiana* and evaluation of antibacterial activity. World J. Microbiol. Biotechnol. 38, 196; https://doi.org/10.1007/s11274-022-03393-3 (2022).
24. Saucedo, S. et al. *Moringa* plants: bioactive compounds and promising applications in food products. Food Res. Int. 111, 438–450; https://doi.org/10.1016/j.foodres.2018.05.062 (2018).
25. Islam, Z. et al. *Moringa oleifera* is a prominent source of nutrients with potential health benefits. Int. J. Food Sci. 6627265; https://doi.org/10.1155/2021/6627265 (2021).
26. Nouri, S., Moslehishad, M., Seyede Marzieh Hosseini, S.M., Etemadi, M. Comparison of antioxidant and alpha-glucosidase inhibitory properties of *Moringa Peregrina* and *Ferulago carduchorum* leaf extracts and microencapsulation of superior plant. J. Food Quality 5887180; https://doi.org/10.1155/2022/5887180 (2022).

27. Tadevosyan, A. Hypoglycemic and hypolipidemic activity of *Moringa* grown in hydroponics and soil in Ararat Valley. Func. Foods Health Disease 13, 398–408; https://doi.org/10.31989/ffhd.v13i8.1158 (2023).
28. Kiran, M.S. et al. Green synthesis and characterization of gold nanoparticles from *Moringa oleifera* leaves and assessment of antioxidant, antidiabetic and anticancer properties. Chem. Data Collect. 33, 100714; https://doi.org/10.1016/j.cdc.2021.1007714 (2021).
29. Ezhilarasi, A.A. et al. Green synthesis of NiO nanoparticles using *Moringa oleifera* extract and their biomedical applications: cytotoxicity effect of nanoparticles against HT-29 cancer cells. J. Photochem. Photobiol. B: Biology 164, 352–360; https://doi.org/10.1016/j.jphotobiol.2016.10.003 (2016).
30. Benton Jones Jr., J. Complete Guide for Growing Plants Hydroponically. 223 p.; https://doi.org/10.1201/b16482 (CRC Press, Taylor & Francis Group, 2014).
31. Gevorgyan, S. et al. Structural characterization and antibacterial activity of silver nanoparticles synthesized using a low-molecular-weight *Royal jelly* extract. Sci. Rep.12, 14077; https://doi.org/10.1038/s41598-022-17929-y (2022).
32. Manosalva, N. et al. Green synthesis of silver nanoparticles: effect of synthesis reaction parameters on antimicrobial activity. World J Microbiol. Biotechnol. 35, 88; https://doi.org/10.1007/s11274-019-2664-3 (2019).
33. Razavi, R. et al. Green synthesis of ag nanoparticles in oil-in-water nano-emulsion and evaluation of their antibacterial and cytotoxic properties as well as molecular Docking. Arab. J. Chem. 14, 103323; https://doi.org/10.1016/j.arabjc.2021.103323 (2021).
34. Basta, A.H., Lotfy, V.F., Mahmoud, K., Abdelwahed, N.A.M. Synthesis and evaluation of protein-based biopolymer in production of silver nanoparticles as bioactive compound versus carbohydrates-based biopolymers. R. Soc. Open Sci. 7, 200928; https://doi.org/10.1098/rsos.200928 (2020).
35. Ali, MH. et al. Analysis of crystallographic structures and properties of silver nanoparticles synthesized using PKL extract and nanoscale characterization techniques. ACS Omega. 8, 28133–28142; https://doi.org/10.1021/acsomega.3c01261 (2023).
36. Mohammed, M.G., Hawar, S.N. Green biosynthesis of silver nanoparticles from *Moringa oleifera* leaves and its antimicrobial and cytotoxicity activities. Int. J. Biomat. 4136641; https://doi.org/10.1155/2022/4136641 (2022).
37. Gabrielyan, L., Badalyan, H., Gevorgyan, V., Trchounian A. Comparable antibacterial effects and action mechanisms of silver and iron oxide nanoparticles on *Escherichia coli* and *Salmonella typhimurium*. Sci. Rep. 10, 13145; https://doi.org/10.1038/s41598-020-70211-x (2020).
38. Fair, R.J., Tor, Y. Antibiotics and bacterial resistance in the 21st century. Persp. Med. Chem. 6, 25–64; https://doi.org/10.4137/PMC.S14459 (2014).
39. Nadeem, S.F. et al. Antimicrobial resistance: more than 70 years of war between humans and bacteria. Crit. Rev. Microbiol. 46, 578–599; https://doi.org/10.1080/1040841X.2020.1813687 (2020).
40. Khameneh, B., Iranshahy, M., Soheili, V., Bazzaz, B.S.F. Review on plant antimicrobials: a mechanistic viewpoint. Antimicrob. Resist. Infect. Control 8, 118; https://doi.org/10.1186/s13756-019-0559-6 (2019).
41. Huang, L., Chen, R., Luo, J., Hasa, M., Shu, X. Synthesis of phytonic silver nanoparticles as bacterial and ATP energy silencer. J. Inorg. Biochem. 231, 111802; https://doi.org/10.1016/j.jinorgbio.2022.111802 (2022).
42. Leblanc, D.J. Enterococcus in *The Prokaryotes* (eds. Dworkin, M. et al.) 175–204 (Springer, New York, 2006). https://doi.org/10.1007/0-387-30744-3_6 (2006).
43. Liu, L. et al. Inhibition of the ATP synthase sensitizes *Staphylococcus aureus* towards human antimicrobial peptides. Sci. Rep. 10, 11391; https://doi.org/10.1038/s41598-020-68146-4 (2020).
44. Wei, M, Xiang, Q., Wang, P. Chen, L., Ren, M. Ambivalent effects of dissolved organic matter on silver nanoparticles/silver ions transformation: A review. J Hazard. Mater. 445, 130533; https://doi.org/10.1016/j.jhazmat.2022.130533 (2023).
45. Raja, G. et al. Macromolecular environmental regulation of silver nanoparticles in cancer therapy: A critical review. Cancer 12, 664; https://doi.org/10.3390/cancers12030664 (2020).
46. Kocharyan, M. et al. *Royal Jelly*–mediated silver nanoparticles show promising anticancer effect on HeLa and A549 cells through modulation of the VEGFa/PI3K/Akt/MMP-2 pathway. Appl. Organomet. Chem. 38, e7726. https://doi.org/10.1002/aoc.7726 (2024).
47. Somda, D., Bargul, J.L., Wesonga, J.M., Wachira, S.W. Green synthesis of *Brassica carinata* microgreen silver nanoparticles, characterization, safety assessment, and antimicrobial activities. Sci. Rep. 14, 29273; https://doi.org/10.1038/s41598-024-80528-6 (2024).
48. Liaqat, N., Jahan, N., Anwar, T., Qureshi, H. Green synthesized silver nanoparticles: optimization, characterization, antimicrobial activity, and cytotoxicity study by hemolysis assay. Front. Chem. 10, 952006; https://doi.org/10.3389/fchem.2022.952006 (2022).
49. Ginovyan, M. et al. Screening revealed the strong cytotoxic activity of *Achemilla Smirnovii* and *Hypericum alpestre* ethanol extracts on different cancer cell lines. AIMS Biophys. 10, 12–22; https://doi.org/10.3934/biophy.2023002 (2022).

Acknowledgements

The research was supported by the Higher Education and Science Committee of MESCS of the Republic of Armenia (Research project № 24WS-1F025). The authors would like to acknowledge Dr. A. Tadevosyan (Davtyan Institute of Hydroponics Problems, NAS, Armenia) for supplying plant material, and Dr. Narine Zakaryan (Department of Botany and Mycology, Biology Faculty, Yerevan State University, Armenia) for verification and authentication of plant sample.

Author contributions

A.A., M.T., T.M., and A.H. performed the investigation, data curation, formal analysis, validation, and writing of the original draft. M.G., R.S., and S.A. contributed to the methodology, data curation, visualization, and writing of the original draft. L.G.(1) contributed to conceptualization, supervision, funding acquisition, and writing – review & editing. K.T. and L.G.(2) performed the conceptualization, methodology, writing – review & editing. All authors have read and approved the final version of the manuscript.

Declarations

Competing interests

The authors declare no competing interests.

Additional information

Correspondence and requests for materials should be addressed to A.A. or L.G.